Appendix A-2

Journal Paper: Submitted to *ASCE Journal of Engineering Mechanics*, June 2004
Accepted September 2004

Influence of Implicit Integration Scheme on Prediction of Shear Band Formation

Randall J. Hickman[1] and Marte Gutierrez, M.ASCE[2]

[1]Graduate Student, Dept. of Civil Engineering, Virginia Polytechnic Institute & State University, Blacksburg, VA 24061

[2]Assoc. Professor, Dept. of Civil Engineering, Virginia Polytechnic Institute & State University, Blacksburg, VA 24061

Corresponding address:
Marte Gutierrez, PhD
Civil & Environmental Engineering
Virginia Polytechnic Institute & State University
200 Patton Hall, Blacksburg, VA 24061
Tel: 540-231-6357, Fax: 540-231-7532
E-mail: magutier@vt.edu

Abstract: Implicit integration schemes for elastoplastic constitutive equations have been developed in recent years as an alternative to explicit schemes. The consistent tangent constitutive matrix $\mathbf{D}^{con}$ that results from implicit schemes makes the global stiffness matrix consistent with the implicit integration procedure, and differs from the traditional continuum tangent constitutive matrix $\mathbf{D}^{ep}$ that results from explicit schemes. Onset of strain localization and shear banding has been traditionally predicted using the continuum tangent constitutive matrix. It is shown that different criteria for onset of shear-band formation are obtained depending on whether $\mathbf{D}^{con}$ or $\mathbf{D}^{ep}$ is used. It is shown that shear band prediction using $\mathbf{D}^{con}$ is step-size dependent, and that the use of $\mathbf{D}^{con}$ influences the predicted onset of strain localization in frictional materials. An analytical equation for prediction of the onset of shear-band formation using $\mathbf{D}^{con}$ for the Mohr-Coulomb model is developed, and a numerical example is presented.

CE database subject headings: Bifurcations; Constitutive models; Elastoplasticity; Localization

Introduction

The use of implicit integration schemes to solve for elastoplastic response of geomaterials has increased in use in recent years (Runesson 1987; Borja and Lee 1990; Jeremic and Sture 1997; Manzari and Nour 1997). The main feature of implicit algorithms is the use of the final stress point in the constitutive response in calculating all the relevant derivatives and internal variables required in the constitutive relations (Simo and Taylor 1985; Jeremic and Sture 1997). Since this point is not known in advance, a set of Newton iterations is used to advance the solution toward the final point for each load increment. In comparison, explicit integration schemes use the initial stress point to determine the derivatives and internal variables required to form the constitutive relations. Since a solution is assumed to exist, implicit methods generally guarantee that a converged solution will be obtained on the constitutive level, even for highly nonlinear models (Ortiz and Popov 1985). The resulting discretized constitutive relation obtained using implicit schemes is called the consistent tangent operator or the consistent tangent constitutive matrix $\mathbf{D}^{con}$, and differs considerably from the continuum tangent constitutive matrix $\mathbf{D}^{ep}$ obtained using explicit schemes. A compact expression of $\mathbf{D}^{con}$ was obtained by Jeremic and Sture (1997).

In finite element analysis, the use of consistent tangent matrix $\mathbf{D}^{con}$ and implicit integration schemes is fast becoming the preferred method in implementing many types of elastoplastic constitutive models for any local integration scheme (Miehe 1996; Alfano and Rosati 1998; Perez-Fouget et al. 2001; Jirasek and Patzak 2002). The main motivation is that the use of $\mathbf{D}^{con}$ to form the global stiffness matrix for a finite element assemblage preserves the quadratic convergence of the iterative global convergence method, and thus achieves faster convergence in finite element calculations than the use of $\mathbf{D}^{ep}$ (Simo and Taylor 1985). $\mathbf{D}^{ep}$ evaluates the

gradients to the yield surface and to the plastic potential surface at the same stress point, namely the initial stress point. In comparison, $\mathbf{D}^{con}$ is formulated to be consistent with the integration method, and so evaluates the gradients to the yield surface and to the plastic potential surface at different stress points. Therefore, $\mathbf{D}^{con}$ is generally non-symmetric even when applied to models with associated flow rules. In contrast, $\mathbf{D}^{ep}$ is only non-symmetric for non-associated flow.

Non-symmetry of the constitutive matrix **D** causes the acoustic tensor **B** (defined below) to become non-positive definite and produces negative eigenvalues for certain wave propagation directions. In bifurcation theory, such negative eigenvalues imply strain localization and instability, following Mandel's (1964) stability criterion. It is to be noted that Mandel's criterion is a necessary and sufficient criterion to detect the onset of instability in material. As a result of non-symmetry in the constitutive and/or global stiffness matrices, localized deformations may occur during finite element calculations. Localization of deformation is extensively observed in many geomaterials subjected to large deformations. The most common type of localized deformation in geomaterials is the shear band, although other types of localized deformation such as the compaction band and dilation band are also observed and may be predicted (Olsson 1999; Issen and Rudnicki 2000; DuBernard et al. 2002; Issen and Challa 2003). The localization of deformation was first treated as a bifurcation problem by Rudnicki and Rice (1975), in which a material undergoing homogenous deformation reaches a bifurcation point, experiences material instability, and deformation becomes non-homogenous. Extensive experimental studies have been performed on frictional-cohesive geomaterials by Arthur et al. (1977), Ord et al. (1991), Besuelle (2001), and Lade (2002), among others, and have shown that shear bands can form before the peak strength of material is mobilized.

Numerous analytical and numerical studies have been performed to simulate various phenomena observed during strain localization: these include efforts to promote strain localization by introducing vertex-like areas to the yield surface (Rudnicki and Rice 1975; Bardet 1991), and efforts to simulate strain localization in finite element structures using gradient plasticity (Bazant and Pijaudier-Cabot 1988; deBorst and Muhlhaus 1992) and Cosserat continua (deBorst 1991).

A review of the different studies that have been performed so far reveals that, as yet, implicit integration schemes and their effects on prediction of shear band formation have not been investigated. This is despite the fact that implicit schemes are now gaining wide acceptance and use in constitutive and finite element modeling. Three properties of $\mathbf{D}^{con}$ may affect the prediction of shear band formation. These properties include: 1) non-symmetry for associated flow, 2) reduced stiffness, and 3) step-size dependence. The effects of using $\mathbf{D}^{con}$ instead of $\mathbf{D}^{ep}$ to predict the onset of strain localization are investigated in this paper.

The objective of this paper is to show the effects of using implicit integration schemes in predicting the onset of strain localization in frictional-cohesive geomaterials. This article is concerned only with the conditions for instability in a geomaterial and the ability to predict the onset of instability and shear band formation using constitutive equations. Simulation of post-localization or post-bifurcation material response is not addressed.

General Equations

Background information related to this work is presented in this section. These include a description of implicit integration schemes and the elastoplastic constitutive matrix, and a description of bifurcation theory and its use to predict the onset of strain localization using the elastoplastic constitutive matrix and the acoustic tensor.

Implicit Integration Schemes and the Elastoplastic Constitutive Matrix

Constitutive relations for most elastoplastic models are given by following set of equations:

$$d\varepsilon_{ij} = d\varepsilon_{ij}^{e} + d\varepsilon_{ij}^{p} \tag{1}$$

$$d\sigma_{ij} = D_{ijkl}^{e} d\varepsilon_{kl}^{e} \tag{2}$$

$$d\varepsilon_{ij}^{p} = \lambda \frac{\partial g}{\partial \sigma_{ij}} \tag{3}$$

$$dq_{\alpha} = \lambda h_{\alpha} \tag{4}$$

where $d\varepsilon_{ij}$, $d\varepsilon_{ij}^{e}$, and $d\varepsilon_{ij}^{p}$ are the increments of the total, elastic, and plastic strain tensors; $d\sigma_{ij}$ is the increment of the Cauchy stress tensor; D_{ijkl}^{e} is the elastic constitutive tensor; λ is the plastic multiplier; $\partial g / \partial \sigma_{ij}$ is the gradient to the plastic potential surface; q_{α} is the set of plastic hardening variables; and h_{α} is the plastic hardening rule. Eqs. (1) to (4) represent the properties of strain additivity, incremental elasticity, plastic flow rule, and plastic hardening rule, respectively.

Eqs. (1) to (3) may be combined into a single equation to solve for the stress increment $d\sigma_{ij}$ for a given strain increment $d\varepsilon_{ij}$:

$$d\sigma_{ij} = D_{ijkl}^{e} \left(d\varepsilon_{kl} - \lambda \frac{\partial g}{\partial \sigma_{ij}} \right) \tag{5}$$

Implementation of the constitutive model requires the numerical integration of Eqs. (1) to (4). For rate-independent elastoplasticity, the values of f and λ are restricted by the Kuhn-Tucker loading-unloading criterion:

$$f(\sigma_{ij}, q_{\alpha}) = 0 \tag{6}$$

$$\lambda \geq 0 \tag{7}$$

$$f\lambda = 0 \tag{8}$$

Eqs. (6) to (8) must be satisfied simultaneously for all loading conditions. Eq. (6) specifies that the yield function must be non-positive for any set of stresses and hardening variables. For elastoplastic loading, the stress point must lie on the yield surface at all stages of loading, which generally requires that plastic strain occurs and $\lambda > 0$. The goal of a numerical calculation for an elastoplastic loading step is to find the correct value of λ such that the final stress point is consistent with the final yield surface ($f = 0$). Using Eqs. (4) and (5) to satisfy Eq. (6):

$$\begin{aligned} f(\sigma_{ij,f}, q_{\alpha,f}) &= f(\sigma_{ij,0} + d\sigma_{ij}, q_{\alpha,0} + dq_{\alpha}) \\ &= f\left(\sigma_{ij,0} + D^{e}_{ijkl}\left(d\varepsilon_{kl} - \lambda \frac{\partial g}{\partial \sigma_{kl}} \right), q_{\alpha,0} + \lambda h_{\alpha} \right) = 0 \end{aligned} \tag{9}$$

For linear elastic models, the plastic flow direction is the only quantity in Eq. (9) that depends on the loading increment and continuously evolves during loading. An additional complication arises from nonlinear elasticity, where the elastic moduli also evolve during a finite loading increment. Borja (1991) showed how to use secant elastic moduli with an implicit integration scheme for such models. Implicit numerical integration schemes for elastoplasticity satisfy Eq. (9) by using the plastic flow direction at the final stress point $\sigma_{ij,f}$:

$$\frac{\partial g}{\partial \sigma_{ij,f}} = \left. \frac{\partial g}{\partial \sigma_{ij}} \right|_{\sigma_{ij,f}} \tag{10}$$

Implicit integration schemes continually update the trial value of λ and the trial plastic flow direction during the iterative solution process. As described by Jeremic and Sture (1997), an approximate solution for the final plastic flow direction is attained readily as a function of the derivatives of the plastic flow direction by using the first two terms of the Taylor series

expansion of Eq. (10), evaluated at the initial stress point $\sigma_{ij,0}$:

$$\frac{\partial g}{\partial \sigma_{ij,f}} = \left.\frac{\partial g}{\partial \sigma_{ij}}\right|_{\sigma_{ij,f}} \approx \left.\frac{\partial g}{\partial \sigma_{ij}}\right|_{\sigma_{ij,0}} + \left(\left.\frac{\partial^2 g}{\partial \sigma_{ij}\partial \sigma_{kl}}\right|_{\sigma_{ij,0}}\right) d\sigma_{kl} + \left(\left.\frac{\partial^2 g}{\partial \sigma_{ij}\partial q_\alpha}\right|_{\sigma_{ij,0}}\right) dq_\alpha \tag{11}$$

For finite element calculations, it is necessary to form a global stiffness matrix to calculate displacements for the next loading step or global iteration. The global stiffness matrix is formed using an elastoplastic constitutive matrix, which is either the continuum tangent constitutive matrix $\mathbf{D}^{ep}$ or the consistent tangent constitutive matrix $\mathbf{D}^{con}$. $\mathbf{D}^{con}$ has been shown to promote faster global convergence, as discussed earlier. These two constitutive matrices and their differences in final form are discussed below.

Both $\mathbf{D}^{ep}$ and $\mathbf{D}^{con}$ are formed by combining Eq. (5) and Prager's consistency condition:

$$df = \frac{\partial f}{\partial \sigma_{ij}} d\sigma_{ij} + \frac{\partial f}{\partial q_\alpha} dq_\alpha \tag{12}$$

Ultimately, both $\mathbf{D}^{ep}$ and $\mathbf{D}^{con}$ are formed using the difference between the elastic and plastic tangent matrices:

$$D^{ep}_{ijkl} = D^{e}_{ijkl} - D^{p}_{ijkl} = D^{e}_{ijkl} - \frac{D^{e}_{ijmn}\dfrac{\partial g}{\partial \sigma_{mn,0}}\dfrac{\partial f}{\partial \sigma_{pq}} D^{e}_{pqkl}}{\dfrac{\partial f}{\partial \sigma_{rs}} D^{e}_{rstu}\dfrac{\partial g}{\partial \sigma_{tu,0}} - \dfrac{\partial f}{\partial q_\alpha} h_\alpha} = D^{e}_{ijkl} - \frac{D^{e}_{ijmn}\dfrac{\partial g}{\partial \sigma_{mn,0}}\dfrac{\partial f}{\partial \sigma_{pq}} D^{e}_{pqkl}}{H_p + H} \tag{13a}$$

$$D^{con}_{ijkl} = R^{e}_{ijkl} - R^{p}_{ijkl} = R^{e}_{ijkl} - \frac{R^{e}_{ijmn}\dfrac{\partial m}{\partial \sigma_{mn}}\dfrac{\partial f}{\partial \sigma_{pq}} R^{e}_{pqkl}}{\dfrac{\partial f}{\partial \sigma_{rs}} R^{e}_{rstu}\dfrac{\partial m}{\partial \sigma_{tu}} - \dfrac{\partial f}{\partial q_\alpha} h_\alpha} = R^{e}_{ijkl} - \frac{R^{e}_{ijmn}\dfrac{\partial m}{\partial \sigma_{mn}}\dfrac{\partial f}{\partial \sigma_{pq}} R^{e}_{pqkl}}{H_p + H} \tag{13b}$$

where $\partial m/\partial \sigma_{ij}$ is a modified plastic flow direction that incorporates the projected change in hardening parameter, H_p is the perfectly plastic modulus, H is the plastic hardening modulus, and R^{e}_{ijkl} is a modified stiffness tensor that Jeremic and Sture (1997) call the "reduced stiffness

tensor". The following expressions for H_p are obtained for $\mathbf{D}^{ep}$ and $\mathbf{D}^{con}$:

$$H_p = \frac{\partial f}{\partial \sigma_{rs}} D^e_{rstu} \frac{\partial g}{\partial \sigma_{tu,0}} \quad \text{for } \mathbf{D}^{ep} \quad \text{and} \quad H_p = \frac{\partial f}{\partial \sigma_{rs}} R^e_{rstu} \frac{\partial m}{\partial \sigma_{tu}} \quad \text{for } \mathbf{D}^{con} \tag{14}$$

Both $\mathbf{D}^{ep}$ and $\mathbf{D}^{con}$ can be expressed in a single general form:

$$\left\{D^{ep}_{ijkl}, D^{con}_{ijkl}\right\} = E^e_{ijkl} - \frac{E^e_{ijmn} Q_{mn} \dfrac{\partial f}{\partial \sigma_{pq}} E^e_{pqkl}}{\dfrac{\partial f}{\partial \sigma_{rs}} E^e_{rstu} Q_{tu} - \dfrac{\partial f}{\partial q_\alpha} h_\alpha} = E^e_{ijkl} - \frac{E^e_{ijmn} Q_{mn} \dfrac{\partial f}{\partial \sigma_{pq}} E^e_{pqkl}}{H_p + H} \tag{15}$$

In Eq. (15), E^e_{ijkl} is a general expression for the elastic constitutive matrix and Q_{ij} is a general expression for the plastic flow direction. The final forms of $\mathbf{D}^{ep}$ and $\mathbf{D}^{con}$ are not the same due to the differences between E^e_{ijkl} and Q_{ij}, as shown by Jeremic and Sture (1997) and as summarized in Table 1.

Several differences between $\mathbf{D}^{ep}$ and $\mathbf{D}^{con}$ may be noted. First, the terms used to form $\mathbf{D}^{ep}$ are constant at a given stress point, while the terms used to form $\mathbf{D}^{con}$ are functions of the magnitude of λ from the previous loading step. Since the magnitude of λ depends on the magnitude of the loading step, $\mathbf{D}^{con}$ is step-size-dependent, while $\mathbf{D}^{ep}$ is step-size-independent. Jeremic and Sture (1997) show that $\mathbf{D}^{con}$ converges to $\mathbf{D}^{ep}$ as $\lambda \rightarrow 0$, or for an infinitesimally small elastoplastic loading step. Second, the terms $Q_{mn} = \partial g / \partial \sigma_{mn}$ and $\partial f / \partial \sigma_{pq}$ in Eq. (15) are equal for associated flow, so $D^{ep}_{ijkl} = D^{ep}_{klij}$ and $\mathbf{D}^{ep}$ is symmetric for associated flow. In contrast, the terms $Q_{mn} = \partial g / \partial \sigma_{mn} + \lambda \, \partial^2 g / (\partial \sigma_{mn} \partial q_\alpha)$ and $\partial f / \partial \sigma_{pq}$ in Eq. (15) are not equal for associated flow, so $D^{ep}_{ijkl} \neq D^{ep}_{klij}$ and $\mathbf{D}^{con}$ is generally non-symmetric even for associated flow. A third difference between $\mathbf{D}^{ep}$ and $\mathbf{D}^{con}$ is that the material stiffness is reduced when $\mathbf{D}^{con}$ is used, as will be demonstrated later.

Since $\mathbf{D}^{con}$ aims to satisfy the constitutive response at the final stress point, its elements may be viewed as local consistent tangent moduli between the initial and final stress point. In contrast, $\mathbf{D}^{ep}$ may be viewed as a tangential matrix since its components are based on the derivatives at the current stress point. This difference between $\mathbf{D}^{ep}$ and $\mathbf{D}^{con}$ is shown schematically in Fig. 1.

Bifurcation and Shear Band Formation

Bifurcation theory is concerned with the prediction of how instability leads to localized deformations in elastoplastic materials. Strain localization manifests itself in cohesive-frictional materials as a narrow zone in which the deformation rate exceeds that in the uniformly deformed material. Since the yielding mechanism for these materials is shearing, the zone of strain localization is called a shear band.

Prediction of strain localization is based on Mandel's (1964) stability criterion which states that a material is stable only when it is able to propagate small perturbations in the form of waves. Instability and strain localization occur when a small perturbation in the form of a wave cannot be propagated across a material in a given direction n_i (i = 1,2,3). This condition appears when the acoustic tensor **B** has a zero or negative determinant, becomes non-positive definite, and produces negative eigenvalues. This condition may be stated for the case in which co-rotational terms are neglected as:

$$\left|B_{ik}\right| = \left|n_j D_{ijkl} n_l\right| \leq 0 \tag{16}$$

B_{ik} is a function of the constitutive matrix **D** and of the direction of wave propagation **n**. The shear band orientation is normal to **n**, as shown in Fig. 2.

For the two-dimensional, plane strain condition (i,j,k,l = 1,2), **D** may be expressed as a 3x3 matrix by deleting from the three-dimensional constitutive matrix the components which

correspond to out-of-plane straining:

$$D_{ijkl} = \begin{bmatrix} D_{1111} & D_{1122} & D_{1112} \\ D_{2211} & D_{2222} & D_{2212} \\ D_{1211} & D_{1222} & D_{1212} \end{bmatrix} \tag{17}$$

In two dimensions, the unit vector **n** may be expressed in terms of the angle θ between the shear band and the coordinate axes (*i.e.*, between the normal to **n** and the *x*-axis):

$$n_i = \begin{Bmatrix} n_1 \\ n_2 \end{Bmatrix} = \begin{Bmatrix} \sin\theta \\ \cos\theta \end{Bmatrix} \tag{18}$$

The determinant $|\mathbf{B}|$ may then be expressed in terms of D_{ijkl} and θ as:

$$\begin{aligned} |\mathbf{B}| = {} & (\sin^4\theta)(D_{1111}D_{1212} - D_{1112}D_{1211}) + (\cos^4\theta)(D_{1212}D_{2222} - D_{1222}D_{2212}) \\ & + (\sin^3\theta\cos\theta)(D_{1111}D_{1222} + D_{1111}D_{2212} - D_{1122}D_{1211} - D_{1112}D_{2211}) \\ & + (\sin^2\theta\cos^2\theta)\begin{pmatrix} D_{1111}D_{2222} + D_{1112}D_{1222} + D_{1211}D_{2212} \\ - D_{1122}D_{2211} - D_{1122}D_{1212} - D_{1212}D_{2211} \end{pmatrix} \\ & + (\sin\theta\cos^3\theta)(D_{1112}D_{2222} + D_{1211}D_{2222} - D_{1222}D_{2211} - D_{1122}D_{2212}) \end{aligned} \tag{19}$$

If the coordinate axes are aligned with the directions of the major and minor principal stresses as shown in Fig. 2b, the cross-terms (*i.e.*, the terms between normal stresses and shearing strains, and between shearing stresses and normal strains) in the elastoplastic constitutive matrix disappear; that is, $D_{1112} = D_{1211} = D_{2122} = D_{2212} = 0$. This change greatly simplifies Eq. (19):

$$\begin{aligned} |\mathbf{B}| = {} & (\sin^4\theta)(D_{1111}D_{1212}) + (\cos^4\theta)(D_{1212}D_{2222}) \\ & + (\sin^2\theta\cos^2\theta)(D_{1111}D_{2222} - D_{1122}D_{2211} - D_{1122}D_{1212} - D_{1212}D_{2211}) \end{aligned} \tag{20}$$

This result was first reported by Pietruszczak and Bardet (1987).

As seen in Eqs. (12) to (15), the elastoplastic stiffness matrix is a function of *H*. The determinant $|\mathbf{B}|$ may become zero for certain values of *H* and orientations θ. The hardening modulus corresponding to $|\mathbf{B}| = 0$ is obtained by setting Eq. (20) equal to zero and solving for *H* (Bardet 1991). For $\mathbf{D}^{ep}$, *H* is obtained as:

$$H\left(\mathbf{D}^{ep}\right)=\frac{2G}{1-\nu}\left(\begin{array}{l}-\sin^4\theta\left(\dfrac{\partial g}{\partial\sigma_{11}}-\dfrac{\partial g}{\partial\sigma_{22}}\right)\left(\dfrac{\partial f}{\partial\sigma_{11}}-\dfrac{\partial f}{\partial\sigma_{22}}\right)\\ +\sin^2\theta\left(\dfrac{\partial g}{\partial\sigma_{11}}\left(\dfrac{\partial f}{\partial\sigma_{11}}-\dfrac{\partial f}{\partial\sigma_{22}}\right)+\dfrac{\partial f}{\partial\sigma_{11}}\left(\dfrac{\partial g}{\partial\sigma_{11}}-\dfrac{\partial g}{\partial\sigma_{22}}\right)\right)\\ -\dfrac{\partial g}{\partial\sigma_{11}}\dfrac{\partial f}{\partial\sigma_{11}}+\dfrac{(1-\nu)}{2}\dfrac{\partial g}{\partial\sigma_{12}}\dfrac{\partial f}{\partial\sigma_{12}}\end{array}\right) \tag{21}$$

where G is the shear modulus and ν is Poisson's ratio. If the coordinate axes are aligned with the major and minor principal stress directions, the major principal stress $\sigma_1=\sigma_{11}$, the minor principal stress $\sigma_3=\sigma_{22}$, and the shear stress $\sigma_{12}=\partial f/\partial\sigma_{12}=\partial g/\partial\sigma_{12}=0$. The critical angle θ_c at which H is minimized may be found by differentiating Eq. (21) with respect to θ, setting the derivative equal to zero, and solving for $\theta=\theta_c$. The resulting expression for θ_c is:

$$\theta_c\left(\mathbf{D}^{ep}\right)=\sin^{-1}\sqrt{\frac{\dfrac{\partial g}{\partial\sigma_1}\left(\dfrac{\partial f}{\partial\sigma_1}-\dfrac{\partial f}{\partial\sigma_3}\right)+\dfrac{\partial f}{\partial\sigma_1}\left(\dfrac{\partial g}{\partial\sigma_1}-\dfrac{\partial g}{\partial\sigma_3}\right)}{2\left(\dfrac{\partial g}{\partial\sigma_1}-\dfrac{\partial g}{\partial\sigma_3}\right)\left(\dfrac{\partial f}{\partial\sigma_1}-\dfrac{\partial f}{\partial\sigma_3}\right)}} \tag{22}$$

Substituting Eq. (22) into Eq. (21) yields the expression for H_c as:

$$H_c\left(\mathbf{D}^{ep}\right)=\frac{G}{2(1-\nu)}\left[\frac{\left(\dfrac{\partial g}{\partial\sigma_1}\dfrac{\partial f}{\partial\sigma_3}-\dfrac{\partial f}{\partial\sigma_1}\dfrac{\partial g}{\partial\sigma_3}\right)^2}{\left(\dfrac{\partial g}{\partial\sigma_1}-\dfrac{\partial g}{\partial\sigma_3}\right)\left(\dfrac{\partial f}{\partial\sigma_1}-\dfrac{\partial f}{\partial\sigma_3}\right)}\right] \tag{23}$$

The expression for $\mathbf{D}^{con}$ is much more algebraically complicated than the expression for $\mathbf{D}^{ep}$. As such, deriving a general expression for H_c at which strain localization emerges is difficult or impossible in the general case. However, expressions for H_c may be derived for specific constitutive models. An example is shown in the following section.

Application to the Mohr-Coulomb Model

The effect of the form of the elastoplastic constitutive matrix on shear band formation is investigated analytically in this section using the strain hardening Mohr-Coulomb model. Shear band formation is predicted using both $\mathbf{D}^{ep}$ and $\mathbf{D}^{con}$. The Mohr-Coulomb model has the

following yield and plastic potential functions in *p*-*q* space:

$$f = q - p\sin\phi - c\cos\phi \tag{24}$$

$$g = q - p\sin\psi + b \tag{25}$$

where ϕ is the friction angle, c is the cohesion, ψ is the dilatancy angle, and b is a constant which makes the plastic potential equal to zero at the point of interest. The stress invariants p and q represent the mean stress and deviatoric stress, respectively, and are defined as follows in two dimensions:

$$p = \frac{1}{2}\sigma_{ii} = \frac{1}{2}(\sigma_1 + \sigma_3) \tag{26}$$

$$q = \sqrt{\frac{1}{2}s_{ij}s_{ij}} = \frac{1}{2}(\sigma_1 - \sigma_3) \tag{27}$$

where $s_{ij} = \sigma_{ij} - p\delta_{ij}$ is the stress deviator tensor (δ_{ij} is the Kronecker delta).

In terms of the invariants p and q, the critical orientation $\theta_c(\mathbf{D}_{ep})$ in Eq. (22) and the critical hardening modulus $H_c(\mathbf{D}^{ep})$ in Eq. (23) can be re-written in terms of invariants p and q as (Gutierrez 1998):

$$\theta_c\left(\mathbf{D}^{ep}\right) = \frac{1}{4}\left(\frac{\partial f/\partial p}{\partial f/\partial q} + \frac{\partial g/\partial p}{\partial g/\partial q}\right) \tag{28}$$

$$H_c\left(\mathbf{D}^{ep}\right) = \frac{E}{16(1-\nu^2)}\left(\frac{\partial f/\partial p}{\partial f/\partial q} - \frac{\partial g/\partial p}{\partial g/\partial q}\right)^2 = \frac{G}{8(1-\nu)}\left(\frac{\partial f/\partial p}{\partial f/\partial q} - \frac{\partial g/\partial p}{\partial g/\partial q}\right)^2 \tag{29}$$

The derivatives of f and g with respect to the invariants p and q can be obtained from Eqs. (24) to (25) as $\partial f/\partial p = -\sin\phi$, $\partial f/\partial q = 1$, $\partial g/\partial p = -\sin\psi$, and $\partial g/\partial q = 1$. Substituting these derivatives in Eq. (29), or using the appropriate derivatives in Eq. (23), yields an expression for H_c corresponding to $\mathbf{D}^{ep}$ for the Mohr-Coulomb model:

$$H_c\left(\mathbf{D}^{ep}\right)=\frac{G(\sin\phi-\sin\psi)^2}{8(1-\nu)} \tag{30}$$

This value of critical hardening modulus was also obtained using a compliance approach by Vermeer (1982). Classical failure corresponds to a condition in which no further hardening is possible, and is represented by the maximum value of the hardening parameter q_α or by a zero value of H. For the case of associated flow ($\phi = \psi$), the critical hardening modulus is equal to zero; shear band formation is suppressed until classical failure occurs.

The corresponding shear band orientation θ_c for $\mathbf{D}^{ep}$ for the Mohr-Coulomb model becomes:

$$\theta_c\left(\mathbf{D}^{ep}\right)=\frac{1}{2}\cos^{-1}\left(\frac{\sin\phi+\sin\psi}{2}\right) \tag{31}$$

Assuming that the difference between ϕ and ψ is fairly small, it is possible to simplify the above equation to:

$$\theta_c\left(\mathbf{D}^{ep}\right)\approx 45^\circ-\frac{\phi+\psi}{4} \tag{32}$$

Eq. (32), which is known as Arthur-Vardoulakis solution, was proposed empirically by Arthur *et al*. (1977) based on experimental results, and was justified theoretically by Vardoulakis (1980). For perfect plasticity (*i.e.*, $H = 0$), two shear band orientations are possible:

$$\theta_c\approx 45^\circ-\frac{\phi}{2} \quad \text{or} \quad \theta_c\approx 45^\circ-\frac{\psi}{2} \tag{33}$$

These orientations correspond, respectively, to the Mohr-Coulomb and Roscoe (1970) solutions. The Mohr-Coulomb and Roscoe solutions are, respectively, the lower and upper bound values of the shear band orientation measured from the σ_1-axis. Experimentally observed shear band orientations in soils lie between these two values (Bardet 1991).

A critical hardening modulus can also be derived for the Mohr-Coulomb model using $\mathbf{D}^{con}$. For the Mohr-Coulomb model, the dilatancy angle is constant and independent of the hardening parameters q_α. In this case, $\partial^2 g/\left(\partial\sigma_{ij}\partial q_\alpha\right)=0$ and $\partial m/\partial\sigma_{ij}=\partial g/\partial\sigma_{ij}$. When the principal stresses are aligned with the coordinate axes, $\mathbf{D}^{con}$ takes the following form:

$$D_{ijkl}^{con}=\begin{bmatrix} D_{1111}^{con} & D_{1122}^{con} & 0 \\ D_{2211}^{con} & D_{2222}^{con} & 0 \\ 0 & 0 & D_{1212}^{con} \end{bmatrix}=\begin{bmatrix} D_{1111}^{ep} & D_{1122}^{ep} & 0 \\ D_{2211}^{ep} & D_{2222}^{ep} & 0 \\ 0 & 0 & D_{1212}^{ep}\left[1+\frac{\lambda G}{q}\right]^{-1} \end{bmatrix}=\begin{bmatrix} D_{1111}^{ep} & D_{1122}^{ep} & 0 \\ D_{2211}^{ep} & D_{2222}^{ep} & 0 \\ 0 & 0 & G\left[1+\frac{\lambda G}{q}\right]^{-1} \end{bmatrix} \quad (34)$$

$$D_{1212}^{con}=D_{1212}^{ep}\left[1+\frac{\lambda G}{q}\right]^{-1}=G\left[1+\frac{\lambda G}{q}\right]^{-1}=G_{ct} \quad (35)$$

As can be seen, $\mathbf{D}^{ep}$ and $\mathbf{D}^{con}$ differ only in terms of D_{1212}. Since $\mathbf{D}^{ep}$ is symmetric in the case of associated flow for any orientation of the reference axes, it can be verified that $\mathbf{D}^{con}$ is symmetric in the case of associated flow if the principal stresses are aligned with the reference axes. Therefore, it is not expected that use of $\mathbf{D}^{con}$ will lead to prediction of shear band formation in the hardening regime for associated models; this behavior is similar to that for $\mathbf{D}^{ep}$.

Because the coordinate axes are aligned with the principal stress directions, the elastoplastic moduli D_{1111}^{con}, D_{1122}^{con}, D_{2211}^{con}, and D_{2222}^{con} relate principal stress increments to principal strain increments. These elastoplastic moduli, which will be called full moduli, are the same for $\mathbf{D}^{con}$ as for $\mathbf{D}^{ep}$. In contrast, any applied stress increment $d\sigma_{12}$ causes principal stress rotation. The stress increment $d\sigma_{12}$ is related only to the elastoplastic modulus D_{1212}^{ep} or D_{1212}^{con} in the elastoplastic matrix. As shown in Eqs. (34) and (35), the elastoplastic modulus D_{1212}^{con} represents a reduced value from D_{1212}^{ep}. The entry D_{1212}^{con} can be thought of as a "reduced" elastoplastic modulus, respectively, in contrast to the full elastoplastic modulus D_{1212}^{ep}, and differs only due to a reduced value of the shear modulus G.

Since $\mathbf{D}^{ep}$ represents the incremental tangent stiffness at the initial stress point and $\mathbf{D}^{con}$ represents the incremental consistent tangent stiffness between the initial stress point and the projected final stress point, G and G_{ct} are the tangent and consistent tangent shear moduli, respectively. G_{ct} is less than G, and therefore promotes a softer response.

An expression for H_c may be derived for $\mathbf{D}^{con}$ in the same way as was done for $\mathbf{D}^{ep}$. Using Eq. (32) to form $\mathbf{D}^{con}$, substituting the resulting expression into Eq. (19), and then solving for H yields the following expression:

$$H\left(\mathbf{D}^{con}\right)=\frac{2GG_{ct}}{G_{ct}\left(1-\nu\right)+2\left(G-G_{ct}\right)\sin^2\theta\cos^2\theta}\left(\begin{array}{l}-\sin^4\theta\left(\dfrac{\partial g}{\partial\sigma_{11}}-\dfrac{\partial g}{\partial\sigma_{22}}\right)\left(\dfrac{\partial f}{\partial\sigma_{11}}-\dfrac{\partial f}{\partial\sigma_{22}}\right)\\ +\sin^2\theta\left(\dfrac{\partial g}{\partial\sigma_{11}}\left(\dfrac{\partial f}{\partial\sigma_{11}}-\dfrac{\partial f}{\partial\sigma_{22}}\right)+\dfrac{\partial f}{\partial\sigma_{11}}\left(\dfrac{\partial g}{\partial\sigma_{11}}-\dfrac{\partial g}{\partial\sigma_{22}}\right)\right)\\ -\dfrac{\partial g}{\partial\sigma_{11}}\dfrac{\partial f}{\partial\sigma_{11}}+\dfrac{\left(1-\nu\right)}{2}\dfrac{\partial g}{\partial\sigma_{12}}\dfrac{\partial f}{\partial\sigma_{12}}\end{array}\right) \tag{36}$$

Comparing Eq. (21) to Eq. (36), it may be seen that that:

$$\frac{H\left(\mathbf{D}^{con}\right)}{H\left(\mathbf{D}^{ep}\right)}=\frac{G_{ct}\left(1-\nu\right)}{G_{ct}\left(1-\nu\right)+\left(G-G_{ct}\right)\sin^2\theta\cos^2\theta} \tag{37}$$

Since the relationship between G and G_{ct} is known, Eq. (37) can be simplified to:

$$\frac{H\left(\mathbf{D}^{con}\right)}{H\left(\mathbf{D}^{ep}\right)}=\frac{1-\nu}{1-\nu+\dfrac{2\lambda G}{q}\sin^2\theta\cos^2\theta} \tag{38}$$

As can be seen, the ratio between the critical hardening moduli for $\mathbf{D}^{ep}$ and $\mathbf{D}^{con}$ is a function of the shear band orientation θ. Although it is possible to differentiate Eq. (36) with respect to θ to find the critical hardening modulus for $\mathbf{D}^{con}$, the resulting expression is very complicated and does not provide clear physical insight into the influence of $\mathbf{D}^{con}$ on H_c and θ_c. A simpler approach is obtained if Eq. (32) is used as the expression for the critical angle θ_c for $\mathbf{D}^{con}$. Based on this approximation, the ratio between critical hardening moduli determined

using $\mathbf{D}^{con}$ and $\mathbf{D}^{ep}$ is shown in the following equation:

$$\frac{H_c(\mathbf{D}^{con})}{H_c(\mathbf{D}^{ep})} = \frac{8(1-\nu)}{8(1-\nu)+\frac{\lambda G}{q}\left[4-(\sin\phi+\sin\psi)^2\right]} \tag{39}$$

The use of the shear band orientation from $\mathbf{D}^{ep}$ given in Eq. (31) in the foregoing equation assumes that the expression for the critical angle determined by minimizing the derivative of Eq. (36) is only slightly different from Eq. (22), which was obtained by minimizing the derivative of Eq. (21). The validity of this assumption will be numerically investigated in the next section.

It is seen that the expression in Eq. (39) is always less than or equal to 1. The critical hardening modulus at which strain localization emerges is therefore reduced when $\mathbf{D}^{con}$ is used. H_c ($\mathbf{D}^{con}$) is then:

$$H_c\left(\mathbf{D}^{con}\right) = \frac{G(\sin\phi-\sin\psi)^2}{8(1-\nu)+\frac{\lambda G}{q}\left[4-(\sin\phi+\sin\psi)^2\right]} \tag{40}$$

Since the critical hardening modulus at shear band formation using $\mathbf{D}^{con}$ is less than the critical hardening modulus using $\mathbf{D}^{ep}$, the effect of implicit integration is to decrease the hardening modulus at which shear bands form. Because the hardening modulus for a shearing yield mechanism generally decreases as plastic shear deformation accumulates, the overall effect of using $\mathbf{D}^{ep}$ is to delay shear band formation until the critical hardening modulus is reduced. Note that if $\lambda = 0$, $\mathbf{D}^{con}$ becomes equal to $\mathbf{D}^{ep}$, and the same critical hardening modulus is obtained using either matrix. For associated flow, the critical hardening modulus for both $\mathbf{D}^{con}$ and $\mathbf{D}^{ep}$ is equal to zero, and only classical failure occurs.

Numerical Example

A numerical example is presented to illustrate the different results obtained regarding shear

band prediction by using $\mathbf{D}^{con}$ rather than $\mathbf{D}^{ep}$. The example uses the Mohr-Coulomb model.

As can be seen in Eq. (40), H_c ($\mathbf{D}^{con}$) depends on several parameters. In order to show typical variations of H_c ($\mathbf{D}^{con}$), Eq. (40) is evaluated using the Mohr-Coulomb model with the parameter values given in Table 2. It is noted from Eq. (40) that H_c ($\mathbf{D}^{con}$) depends on the shear stress q which in turn depends on the stress path. To evaluate q, an idealized stress path with a constant mean stress of p=1 MPa is assumed. ϕ is then increased, and the corresponding value of q is calculated by setting the yield criterion f=0 in Eq. (24). The variation of $H_c(\mathbf{D}^{con})$ as function of ϕ and λ is shown in Fig. 3a. Note that $H_c(\mathbf{D}^{ep})$ is equal to $H_c(\mathbf{D}^{con})$ for λ=0. Fig. 3b shows the ratio $H_c(\mathbf{D}^{con})/H_c(\mathbf{D}^{ep})$ as a function of λ and ϕ. H_c increases continuously with increasing ϕ. For a given friction angle, $H_c(\mathbf{D}^{ep})$ decreases with increasing value of λ. The critical hardening modulus calculated using $\mathbf{D}^{con}$ is always less than the critical modulus calculated using $\mathbf{D}^{ep}$. However, the ratio $H_c(\mathbf{D}^{con})/H_c(\mathbf{D}^{ep})$ approaches one as the friction angle is increased. Clearly, the value of H_c that corresponds to the onset of shear banding depends on the value of λ and therefore on the step size.

Strain localization and shear band formation occurs when the material hardening modulus becomes equal to the critical hardening modulus. For this example, the Mohr-Coulomb model is modified by treating ϕ as a hardening parameter and using a hyperbolic strain hardening function. The hyperbolic hardening function defines ϕ as a function of plastic shear strain ε_s^p.

$$\sin\phi = (\sin\phi_p - \sin\phi_o)\frac{\varepsilon_s^p}{A+\varepsilon_s^p} + \sin\phi_o \tag{41}$$

where $\varepsilon_s = \sqrt{2e_{ij}e_{ij}}$ is the shear strain ($e_{ij} = \varepsilon_{ij} - \frac{1}{2}\varepsilon_{kk}\delta_{ij}$ is the deviatoric strain), A is a hardening parameter, and ϕ_o and ϕ_p are the initial and peak friction angles, respectively. This

hardening rule is similar to that suggested by Poorooshasb and Pietruszczak (1985). The material hardening modulus H then becomes:

$$H = p(\sin\phi_p - \sin\phi_o)\frac{A}{\left(A + \varepsilon_s^p\right)^2} = \frac{p}{A}\frac{(\sin\phi_p - \sin\phi)^2}{\sin\phi_p - \sin\phi_o} \tag{42}$$

The hardening modulus continuously decreases as plastic shear strain accumulates and the mobilized friction angle approaches the maximum possible friction angle. The parameters related to the hardening function are assigned the values listed in Table 2.

The results for this example are shown in Fig. 4. Fig. 4a shows that H decreases and H_c increases as ϕ increases with accumulated plastic strain. Localization occurs when H and H_c become equal, and may be solved by setting either Eq. (29) (for $\mathbf{D}^{ep}$) or Eq. (40) (for $\mathbf{D}^{con}$) equal to Eq. (42). Fig. 4a shows the hardening moduli and mobilized friction angles at which the onset of strain localization is predicted using $\mathbf{D}^{ep}$ and $\mathbf{D}^{con}$, and Fig. 4b shows the equivalent plastic shear strains at which localization occurs. If $\mathbf{D}^{ep}$ is used, localization occurs when the mobilized friction angle ϕ increases to 25.5º, or when the plastic shear strain ε_s^p increases to 0.062. If $\mathbf{D}^{con}$ is used, localization occurs at greater values of ϕ and ε_s^p, as shown in Fig. 4b.

Use of $\mathbf{D}^{con}$ thus has the effect of delaying shear band formation when used with the hardening Mohr-Coulomb model. In this example, the use of $\mathbf{D}^{con}$ allows much more plastic shear strain to occur beyond the point at which shear bands form when $\mathbf{D}^{ep}$ is used. If smaller loading steps are used, the corresponding values of λ decrease and the effect of using $\mathbf{D}^{con}$ is not as significant. However, shear banding should always be delayed through the use of $\mathbf{D}^{con}$ in finite element calculations, as loads are usually applied as discrete increments.

Fig. 5 shows the variation of critical angles θ_c obtained from $\mathbf{D}^{con}$ by minimizing the derivative of Eq. (37) with respect to θ, and setting the derivative equal to zero. The predicted

shear band orientations θ_c are plotted against $\phi+\psi$ and for different values of λ. The θ_c values for $\lambda=0$ correspond to values obtained from $\mathbf{D}^{ep}$. As can be seen, the critical angles θ_c at which the shear bands form are only slightly different for both elastoplastic matrices. The differences in θ_c for different values of λ increases with increasing ϕ. However, the maximum variation in shear band orientations for different values of λ does not exceed 1.5° for $\phi=50°$. The critical angles θ_c vary almost linearly with the friction angle ϕ. Also, the predicted variations of θ_c with respect to $\phi+\psi$ are all asymptotic to the straight line $\theta_c=45-(\phi+\psi)/4$, which is identical to the Arthur-Vardoulakis orientation given in Eq. (33).

An interesting observation that can be made from Fig. 5 is that the predicted shear band orientations for $\mathbf{D}^{ep}$ has slightly more deviation from the straight-line $\theta_c=45-(\phi+\psi)/4$ relationship than for $\mathbf{D}^{con}$ with $\lambda>0$. The deviation for $\mathbf{D}^{ep}$ or $\lambda=0$ corresponds to the approximation made in simplifying Eq. (31) and Eq. (32); that is, it is assumed that the difference between ϕ and ψ is fairly small such that $\cos(\phi-\psi)\approx 1$. It can be concluded that the shear band orientations from $\mathbf{D}^{con}$ are actually closer to the Arthur-Vardoulakis orientation than the shear band orientations from $\mathbf{D}^{ep}$. This conclusion validates the assumption made in the use of $\theta=45-(\phi+\psi)/4$ to develop the analytical expression for $H_c(\mathbf{D}^{ep})$ in Eq. (40). It must be noted, however, that although the Arthur-Vardoulakis orientation given in Eq. (32) is valid for both $\mathbf{D}^{ep}$ and $\mathbf{D}^{con}$, bifurcation actually occurs at a higher friction angle for $\mathbf{D}^{con}$ than for $\mathbf{D}^{ep}$. Consequently, use of $\mathbf{D}^{con}$ predicts a lower shear band orientation angle θ than for $\mathbf{D}^{ep}$.

Discussion of Results

The results presented above show that for models with linear yield and plastic potential functions, the use of $\mathbf{D}^{con}$ yields smaller values of H_c at the onset of bifurcation than when using

$\mathbf{D}^{ep}$. For the Mohr-Coulomb model, only the transverse modulus is affected when $\mathbf{D}^{con}$ is used (Eq. 34). The stiffness is reduced in the neutral loading direction as a result of using the consistent tangent matrix. The reduced critical hardening modulus at strain localization has a similar effect to methods used by Rudnicki and Rice (1975), Bardet (1991), Papamichos and Vardoulakis (1995), and Hashiguchi and Tsutsumi (2003) to soften the transverse modulus and promote shear band formation.

Rudnicki and Rice (1975), and Bardet (1991) showed that the use of vertex-like yield and plastic potential surfaces, in addition to having a non-associated flow rule, strongly influence the prediction of strain localization. The effect of having a vertex in the yield surface is to reduce the transverse modulus or the tangential modulus in the neutral loading direction. The reduction of the transverse modulus is equivalent to increasing the plastic deformation predicted by non-vertex models. A consequence of lower value of the critical hardening modulus is that strain localization occurs at a much higher plastic deformation for $\mathbf{D}^{con}$ than for $\mathbf{D}^{ep}$. The plastic shear strain at localization increases with increasing size of load increment. Due to the delay in strain localization, the friction angle corresponding to the critical hardening modulus is higher. Consequently, the shear band orientation (as measured by the deviation between the shear band orientation and σ_1 direction – see Fig. 2a) is smaller for $\mathbf{D}^{con}$ than for $\mathbf{D}^{ep}$.

The above results showing increased shear strain and lower hardening modulus at strain localization, and smaller deviation between shear band orientation and major principal stress directions, are similar to those predicted by Bardet (1991) using a vertex model, Papamichos and Vardoulakis (1995) using a non-coaxial model, and Hashiguchi and Tsutsumi (2003) using a tangential plasticity model. These results are also supported by experimental data (Bardet

1991; Papamichos and Vardoulakis 1995). It is important to emphasize that the above effects of using $\mathbf{D}^{con}$ are only true for models with linear yield and plastic potential functions.

Conclusions

The effects of the use of implicit integration scheme and the consistent tangent constitutive matrix $\mathbf{D}^{con}$ in predicting shear band formation can be summarized as follows:

1) For constitutive models with linear yield and plastic potential functions such as the Mohr-Coulomb model, the use of $\mathbf{D}^{con}$ results in lower values of the critical plastic hardening modulus in comparison to the use of continuum tangent matrix $\mathbf{D}^{ep}$. Consequently, shear band formation occurs at a larger deformation and at higher values of mobilized friction angle for strain hardening materials.
2) For the strain hardening Mohr-Coulomb model, the deviation between predicted shear band orientations and the Arthur-Vardoulakis orientation of $\theta_c=45-(\phi+\psi)/4$ is less using $\mathbf{D}^{con}$ than deviation obtained using $\mathbf{D}^{ep}$. However, for the same critical friction angle the differences between predicted orientations from $\mathbf{D}^{con}$ and $\mathbf{D}^{ep}$ are very small. For models with linear yield and potential functions, shear band orientation (as measured from the deviation between the shear band orientation and σ_1 direction) is smaller for $\mathbf{D}^{con}$ than for $\mathbf{D}^{ep}$ because the friction angle at strain localization is higher for $\mathbf{D}^{con}$ than for $\mathbf{D}^{ep}$.
3) Predicted shear band formation using $\mathbf{D}^{con}$ is step size dependent. The difference in predicted values of hardening modulus, strain and friction angle at strain localization and shear band orientation between $\mathbf{D}^{con}$ and $\mathbf{D}^{ep}$ increases with increasing load increment.
4) Results from models with linear yield and plastic potential functions using $\mathbf{D}^{con}$ are similar to those predicted by other advanced constitutive models such as vertex,

muti-mechanism, non-coaxial, and tangential plasticity models, and are consistent with existing experimental data.

The above results should be considered when using implicit integration techniques in finite element simulation of shear band formation.

Acknowledgment

The study presented in this article was supported by The Petroleum Research Fund, American Chemical Society under Grant No. 40214 -AC 8. This support is gratefully acknowledged.

References

Alfano, G. and Rosati, L. (1998). "A general approach to the evaluation of consistent tangent operators for rate-independent elastoplasticity." *Comp. Meth. Appl. Mech. Eng.*, 167, 75-89.

Arthur, J.F.R., Dunstan, T., Assadi, Q.A.J., and Assadi, A. (1977). "Plastic deformation and failure in granular material." *Géotechnique*, 27(1), 53-74.

Bardet, J.P. (1991). "Orientation of shear bands in frictional soils." *J. Eng. Mech.*, ASCE, 117, 1466-1484.

Bazant, Z.P. and Pijaudier-Cabot, G. (1988). "Nonlocal continuum damage, localization instability and convergence." *J. Appl. Mech.*, 55(2), 287-293.

Besuelle, P. (2001). "Compacting and dilating shear bands in porous rock: Theoretical and experimental conditions." *J. Geophys. Res.*, 106, 13435-13442.

Borja, R.I. (1991). "Cam-clay plasticity, part II: Implicit integration of constitutive equation based on a nonlinear elastic stress predictor." *Comp. Meth. Appl. Mech. Eng.*, 88, 225-240.

Borja, R.I. and Lee, S.R. (1990). "Cam-clay plasticity, part I: Implicit integration of elasto-plastic constitutive relations." *Comp. Meth. Appl. Mech. Eng.*, 78, 49-72.

deBorst, R. (1991). “Numerical modeling of bifurcation and localization in cohesive-frictional materials.” *Pure Appl. Geophys.*, 137 (4), 367-390.

deBorst, R. and Muhlhaus, H.B. (1992). “Gradient-dependent plasticity – formulation and algorithmic aspects.” *Intl. J. Num. Meth. Eng.*, 35(3), 521-539.

DuBernard, X., Eichhubl, P., and Aydin, A. (2002). “Dilation bands: A new form of localized failure in granular media.” *Geophys. Res. Lett.*, 29(24), 2176.

Gutierrez, M. (1998). “Shear band formation in rocks with a curved failure surface.” *Intl. J. Rock Mech. Mining Sci.*, 35(4/5), 447-456.

Hashiguchi, K. and Tsutsumi, S. (2003). “Shear band formation analysis in soils by the subloading surface model with tangential stress rate effect.” *Intl. J. Plasticity*, 19(10), 1651-1677.

Issen, K.A. and Challa, V. (2003). “Conditions for dilation band formation in granular materials.” *Proc. 16th ASCE Eng. Mech. Conf.*, Seattle, Washington, 4 p.

Issen, K.A. and Rudnicki, J.W. (2000). “Conditions for compaction bands in porous rock.” *J. Geophys. Res.*, 105(B9), 21529-21536.

Jeremic, B. and Sture, S. (1997). “Implicit integration in elastoplastic geotechnics.” *Mech. Cohesive-Frictional Matls.*, 2, 165-183.

Jirasek, M. and Patzak, B. (2002). “Consistent tangent stiffness for nonlocal damage models.” *Computers and Structures*, 80(14-15), 1279-1293.

Lade, P.V. (2002). “Instability, shear banding, and failure in granular materials.” *Intl. J. Solids Struct.*, 39, 3337-3357.

Mandel, J. (1964). “Conditions de stabilite et postulat de Drucker.” *Proc. IUTAM Symp. Rheology Soil Mech.*, Grenoble, France, 58-68.

Manzari, M.T. and Nour, M.A. (1997). "On implicit integration of bounding surface plasticity models." *Computers and Structures*, 63(3), 385-395.

Miehe, C. (1996). "Numerical computation of algorithmic (consistent) tangent moduli in large-strain computational inelasticity." *Comp. Meth. Appl. Mech. Eng.*, 134, 223-240.

Olsson, W.A. (1999). "Theoretical and experimental investigation of compaction bands." *J. Geophys. Res.*, 104, 7219-7228.

Ord, A., Vardoulakis, I., and Kajewski, R. (1991). "Shear band formation in Gosford sandstone." *Intl. J. Rock Mech. Mining Sci. Geomech. Abs.*, 28(5), 397-409.

Ortiz, M. and Popov, E.P. (1985). "Accuracy and stability of integration algorithms for elastoplastic constitutive relations." *Intl. J. Num. Meth. Eng.*, 21, 1561-1576.

Papamichos, E. and Vardoulakis, I. (1995). "Shear band formation in sand according to non-coaxial plasticity model." *Géotechnique*, 45(4), 649-661.

Perez-Fouget, A., Rodriguez-Ferran, A., and Huerta, A. (2001). "Consistent tangent matrices for substepping schemes." *Comp. Meth. Appl. Mech. Eng.*, 190, 4627-4647.

Pietruszczak, S. and Bardet, J.P. (1987). "Strain localization in the context of plasticity based soil models." *Proc. 8th Asian Reg. Conf. Soil Mech. Fnd. Eng.*, Kyoto, Japan, 73-76.

Poorooshasb, H.B. and Pietruszczak, S. (1985). "On yielding and flow of sand: a generalized two-surface model." *Computers and Geotechnics*, 1(1), 33-58.

Roscoe, K.H. (1970). "The influence of strain in soil mechanics." *Géotechnique*, 20(2), 129-170.

Rudnicki, J.W. and Rice J.R. (1975). "Conditions for the localization of deformation in pressure-sensitive dilatant materials." *J. Mech. Phys. Solids*, 23, 371-394.

Runesson, K. (1987). "Implicit integration of elastoplastic relations with reference to soils."

Intl. J. Num. Analy. Meth. Geomech., 11, 315-321.

Simo, J.C. and Taylor, R.L. (1985). "Consistent tangent operators for rate-independent plasticity." *Comp. Meth. Appl. Mech. Eng.* 48, 101-118.

Vardoulakis, I. (1980). "Shear band inclination and shear modulus of sand in biaxial tests." *Intl. J. Num. Analy. Meth. Geomech.*,, 12, 155-168.

Vermeer, P.A. (1982). "A simple shear-band analysis using compliances." *Proc. IUTAM Conf. Deform. Failure Granular Matls.*, Delft, Netherlands, 493-499.

List of Tables

Table 1 - Expressions for E^{e}_{ijkl} and Q_{ij} for $\mathbf{D}^{ep}$ and $\mathbf{D}^{con}$.

Table 2 – Model parameters for models used in shear band predictions.

List of Figures

Fig 1. Stress-strain curve illustrating the different stiffness moduli of $\mathbf{D}^{ep}$ and $\mathbf{D}^{con}$.

Fig. 2. Orientation of shear band with respect to principal stress directions (a) in the general case; (b) when the principal stresses are aligned with the coordinate axes. The angle α between the shear band and σ_1 is the same for both cases, but the angle θ is measured from the *x*-axis and depends on the orientation of the reference axes.

Fig. 3. Variation in critical hardening modulus H_c for different elastoplastic tangent matrices using the hardening Mohr-Coulomb model: (a) Value of H_c/G as a function of friction angle ϕ. (b) Ratio $H_c(\mathbf{D}^{con})/H_c(\mathbf{D}^{ep})$ for several values of λ as a function of friction angle ϕ.

Fig. 4. Comparison of strain localization predictions for $\mathbf{D}^{ep}$ and $\mathbf{D}^{con}$ using the hardening Mohr-Coulomb model. Strain localization occurs when hardening modulus and critical hardening modulus become equal; localization occurs at a lesser friction angle when $\mathbf{D}^{ep}$ is used than when $\mathbf{D}^{con}$ is used. (a) Magnified view showing mobilized friction angles at which localization occurs. (b) Onset of strain localization as a function of plastic shear strain. Onset of strain localization is delayed when $\mathbf{D}^{con}$ is used.

Fig. 5. Critical angle θ_c as a function of friction angle ϕ is nearly independent of λ.

Table 1

	If D^{ep} is used:	If D^{con} is used:
E^e_{ijkl}	D^e_{ijkl}	$R^e_{ijkl} = D^e_{mnkl}\left[\delta_{mi}\delta_{nj} + \lambda D^e_{mnpq}\dfrac{\partial^2 g}{\partial\sigma_{pq}\partial\sigma_{ij}}\right]^{-1}$
Q_{ij}	$\dfrac{\partial g}{\partial\sigma_{ij,0}}$	$\dfrac{\partial m}{\partial\sigma_{ij}} = \dfrac{\partial g}{\partial\sigma_{ij,0}} + \lambda\dfrac{\partial^2 g}{\partial\sigma_{ij}\partial q_\alpha}h_\alpha$

Table 2

Parameter	**Unit**	**Value**
Perfectly Plastic Mohr-Coloumb Model		
Shear modulus, G	MPa	30
Poisson's ratio, ν	-	0.30
Dilatancy angle, ψ	º	0
Cohesion, c	MPa	0
Mean stress, p	MPa	1
Additional Parameters for Hardening Mohr-Coloumb Model		
Initial friction angle, ϕ_o	º	0
Maximum friction angle, ϕ_p	º	30
Hardening parameter, A	-	0.001

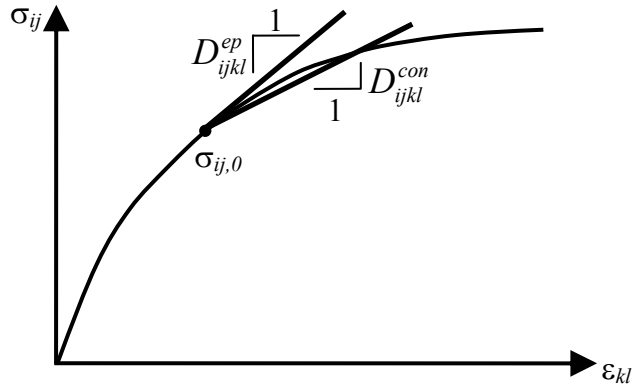
σij
1
Dijklep
1
Dijklcon
σij,0
εkl

Fig. 1

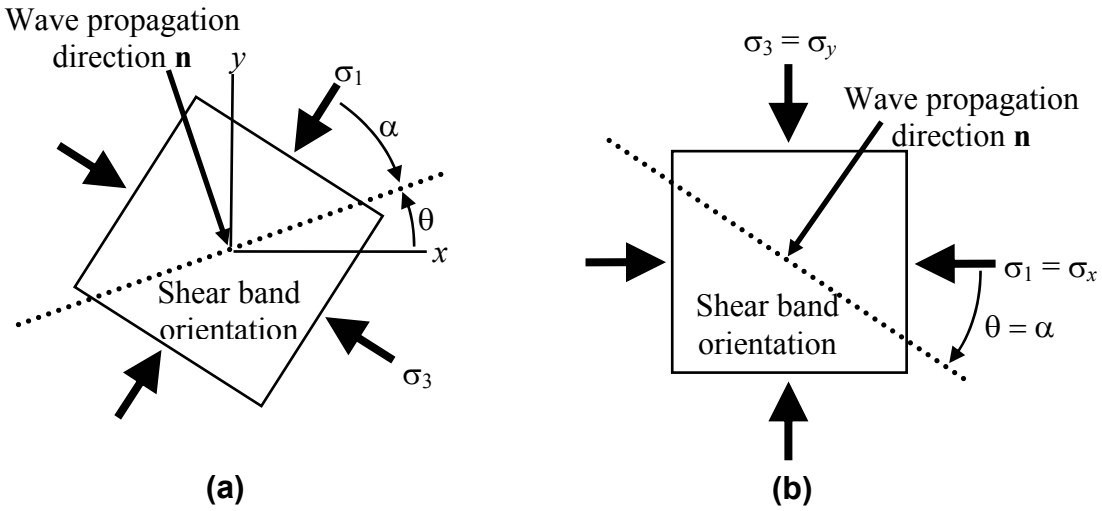
Wave propagation
direction n
y
σ1
α
θ
x
Shear band
orientation
σ3
(a)
σ3 = σy
Wave propagation
direction n
σ1 = σx
Shear band
orientation
θ = α
(b)

Fig 2.

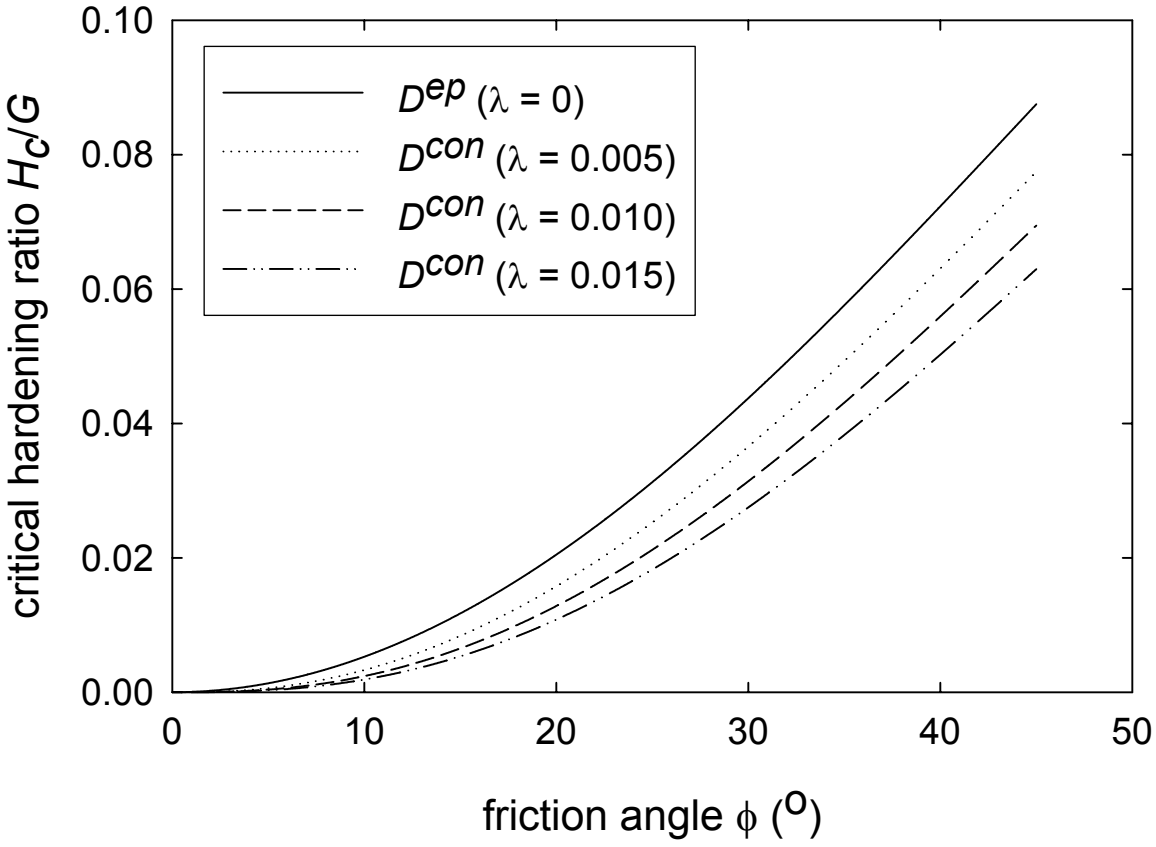
0.10
0.08
0.06
0.04
0.02
0.00
0
10
20
30
40
50
critical hardening ratio H_C/G
friction angle ϕ (^{o})
D^{ep} (λ = 0)
D^{con} (λ = 0.005)
D^{con} (λ = 0.010)
D^{con} (λ = 0.015)

Fig. 3a

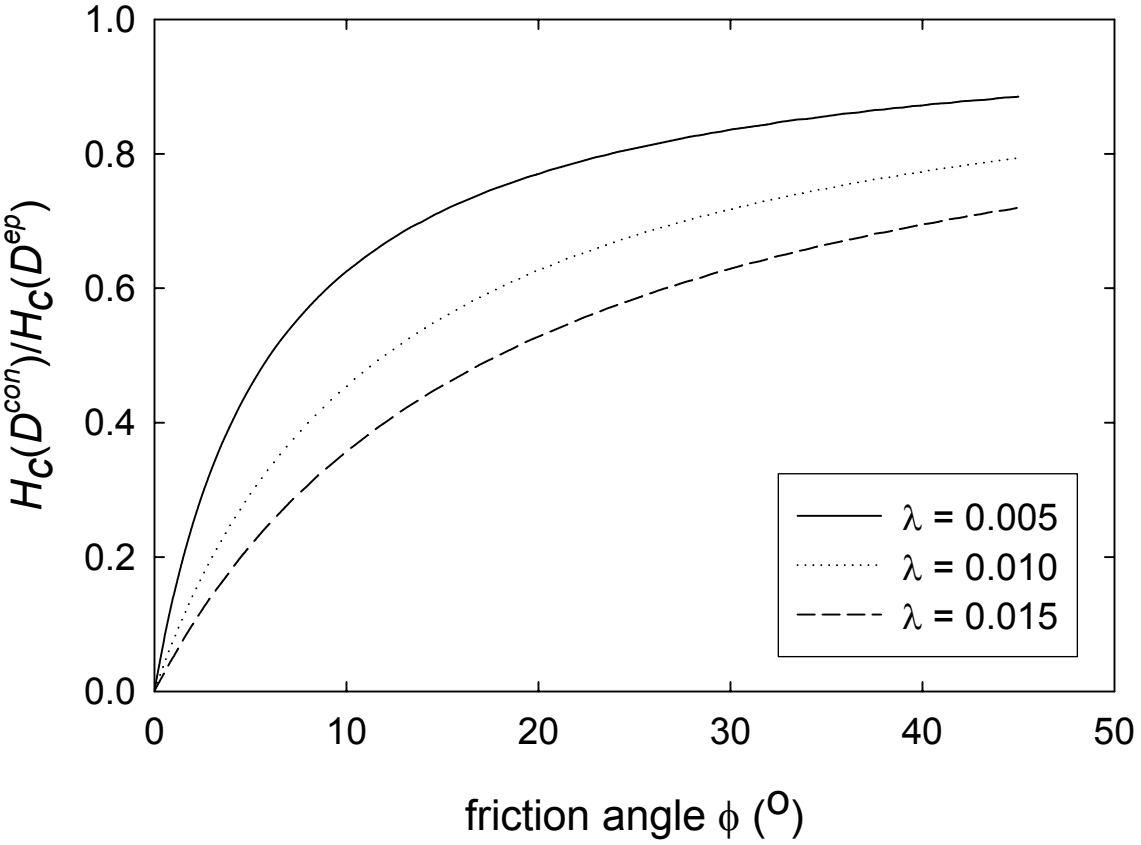
1.0
0.8
0.6
0.4
0.2
0.0
0
10
20
30
40
50
$H_c(D^{con})/H_c(D^{ep})$
friction angle ϕ (^{o})
λ = 0.005
λ = 0.010
λ = 0.015

Fig 3b

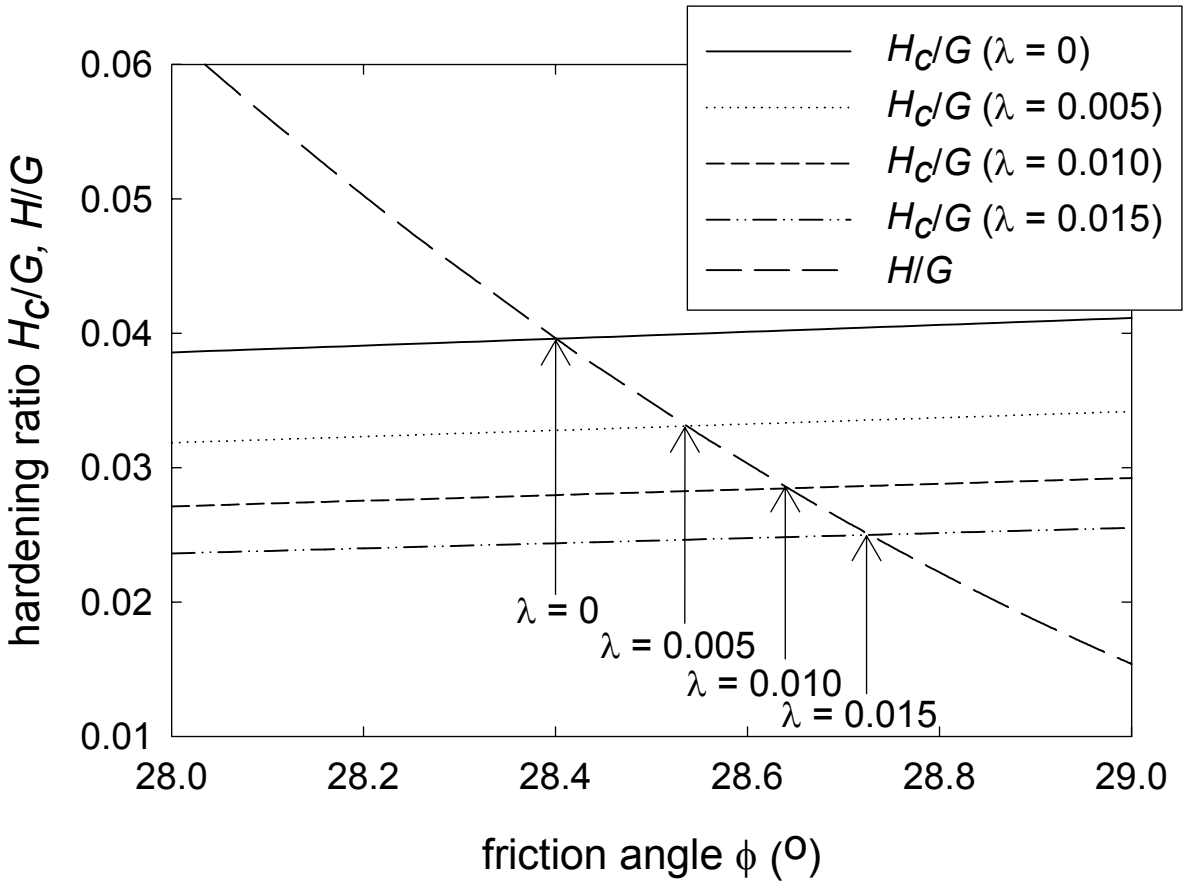
H_C/G (λ = 0)
H_C/G (λ = 0.005)
H_C/G (λ = 0.010)
H_C/G (λ = 0.015)
H/G
hardening ratio H_C/G, H/G
0.06
0.05
0.04
0.03
0.02
0.01
λ = 0
λ = 0.005
λ = 0.010
λ = 0.015
28.0
28.2
28.4
28.6
28.8
29.0
friction angle ϕ (°)

Fig 4a

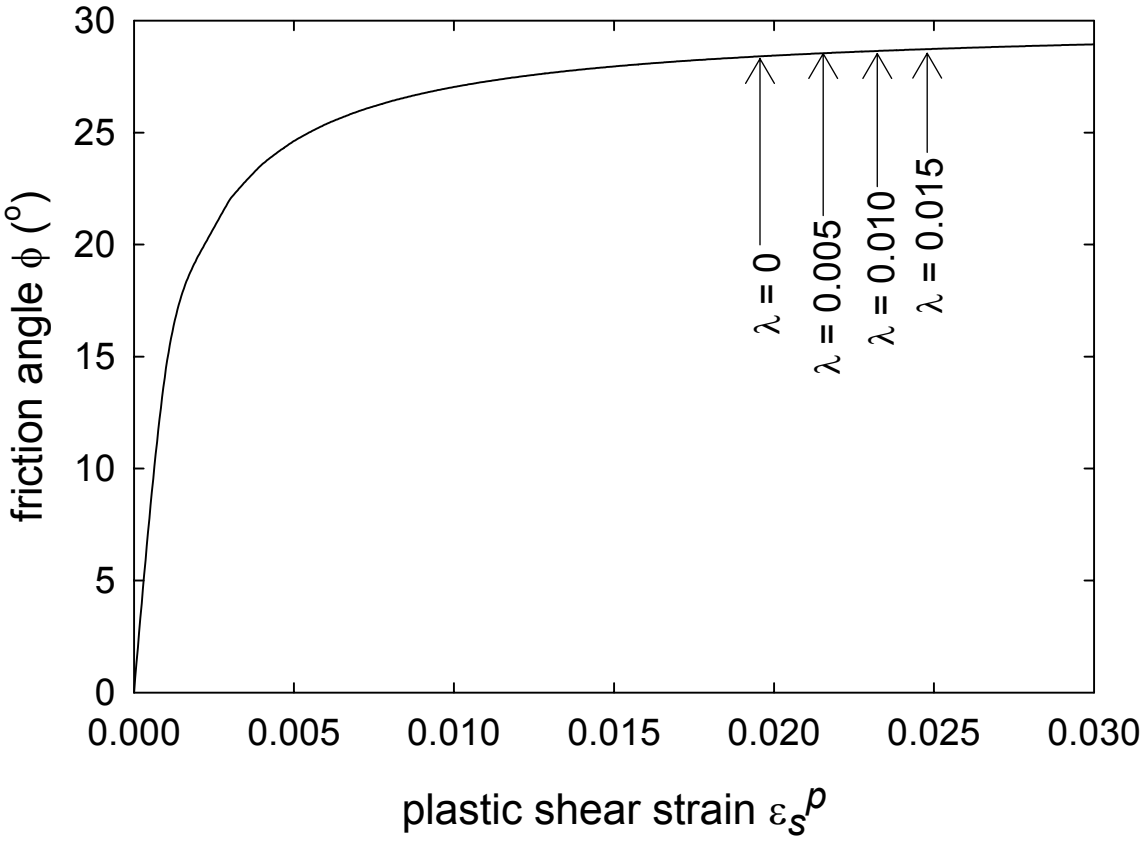
30
25
20
15
10
5
0
0.000
0.005
0.010
0.015
0.020
0.025
0.030
friction angle ϕ (°)
plastic shear strain ε_s^p
λ = 0
λ = 0.005
λ = 0.010
λ = 0.015

Fig. 4b

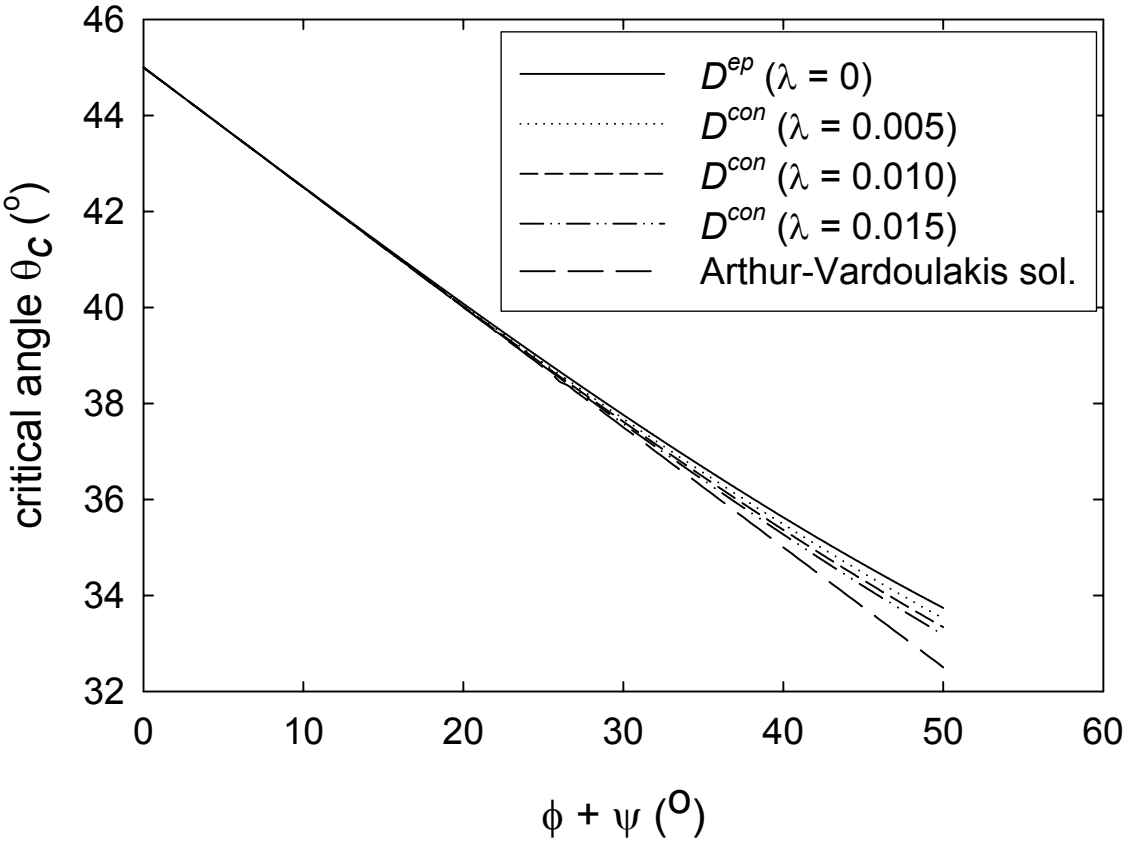
46
44
42
40
38
36
34
32
0
10
20
30
40
50
60
critical angle θc (o)
ϕ + ψ (o)
Dep (λ = 0)
Dcon (λ = 0.005)
Dcon (λ = 0.010)
Dcon (λ = 0.015)
Arthur-Vardoulakis sol.
Fig. 5